Appl. Phys. B 76, 117–124 (2003)
DOI: 10.1007/s00340-002-1073-7

Applied Physics B
Lasers and Optics

A.B. MUNDT
A. KREUTER
C. RUSSO
C. BECHER✉
D. LEIBFRIED*
J. ESCHNER
F. SCHMIDT-KALER
R. BLATT

Coherent coupling of a single $^{40}Ca^{+}$ ion to a high-finesse optical cavity

Institut für Experimentalphysik, Universität Innsbruck, Technikerstraße 25, 6020 Innsbruck, Austria

Received: 23 August 2002
Published online: 8 January 2003 •

ABSTRACT We demonstrate coherent coupling of the quadrupole $S_{1/2} \leftrightarrow D_{5/2}$ optical transition of a single trapped $^{40}Ca^{+}$ ion to the standing wave field of a high-finesse cavity. The dependence of the coupling on temporal dynamics and spatial variations of the intracavity field is investigated in detail. By precisely controlling the position of the ion in the cavity standing wave field and by selectively exciting vibrational state-changing transitions the ion's quantized vibration in the trap is deterministically coupled to the cavity mode. We confirm coherent interaction of ion and cavity field by exciting Rabi oscillations with short resonant laser pulses injected into the cavity, which is frequency-stabilized to the atomic transition.

PACS 32.80.Pj; 03.67.-a; 42.50.Ct

1 Introduction

Laser-cooled trapped atoms or ions are ideally suited systems for the investigation and implementation of quantum information processing [1]. The combination of a Paul-type ion trap [2] with laser cooling leads to unique properties of trapped cold ions, such as localization of the single particle to less than a few tens of nanometers, control of the motional state down to the zero-point of the trapping potential and a high degree of isolation from the environment and thus a very long time available for manipulations and interactions at the quantum level. The very same properties make single trapped atoms and ions well suited for storing quantum information in long-lived internal states, e.g. by encoding a quantum bit (qubit) of information within the coherent superposition of the $S_{1/2}$ ground state and the metastable $D_{5/2}$ excited state of Ca^{+} [3]. However, this stored information is 'spatially static' with respect to transport of quantum information over distances exceeding the trap dimensions. A much better suited carrier of quantum information for fast and reliable transport over long distances are photons. An interface between static and moving qubits requires the controlled coherent interaction of a single atom and a single cavity mode, this being the basic building block for distributed quantum networks [4]. For an experimental implementation of such a scheme one needs to understand and control the dynamics of the atom–cavity coupling. Thus, the demonstration of deterministic *coherent* coupling of a single ionic qubit to one mode of the electromagnetic field inside a high-finesse optical resonator and the detailed investigation of this coupling [5] are of major interest for the implementation of quantum information processing with trapped ions. Deterministic excitation of cavity-induced fluorescence on the short-lived $S_{1/2}$–$P_{1/2}$ dipole transition in Ca^{+} was demonstrated recently, thereby utilizing a single trapped ion as a nanoscopic probe of an optical field [6].

Another application closely related to the atom–photon interface is the triggered emission of single photons from the coupled atom–cavity system [7, 8] or sequences of entangled single-photon wave packets [9]. Efficient deterministic emission of single photons into a well-defined spatial mode is a prerequisite for quantum key distribution [10] and linear optics quantum computation [11].

The ability to precisely place an ion at an arbitrary position within a standing wave (SW) field and the highly orthogonal coupling of different vibrational-state-changing transitions to the SW field can be utilized for cooling the ion's vibrational state well below the Doppler limit [12]. If, in addition, the coupling of atom and cavity mode is strong enough to induce a modification of the atom's spontaneous emission properties [13], one can demonstrate cavity-assisted cooling via destructive quantum interference of heating transitions [14].

Finally, the strong coupling of trapped ions that are cooled to their lowest vibrational state [15, 16] with a quantized cavity field might allow for entangling three quantum subsystems [17, 18], i.e. internal electronic states, quantum vibrational mode and single-mode cavity field.

In this paper we demonstrate important first steps towards the above experiments by coherently coupling the quadrupole $S_{1/2} \leftrightarrow D_{5/2}$ transition of a single trapped Ca^{+} ion to a mode of a high-finesse optical cavity. We investigate the coupling by probing the ion's response to dynamical and spatial variations of the intracavity field. The ion can be placed with high precision at an arbitrary position in the SW field of the cavity. We achieve deterministic coupling of the cavity mode to the ion's vibrational state by selectively exciting state-changing transitions with the cavity light tuned to a vibrational sideband of the $S_{1/2} \leftrightarrow D_{5/2}$ resonance. We prove that the interaction of

✉ E-mail: christoph.becher@uibk.ac.at
**Present address:* Time and Frequency Division, National Institute of Standards and Technology, Boulder, CO 80305, USA

ion and cavity field is coherent by exciting Rabi oscillations through the field in the frequency-stabilized cavity.

2 Experimental setup

2.1 *Trap and cavity setup*

The $^{40}Ca^{+}$ ion is stored in a spherical Paul trap [2] placed in the center of a near-confocal resonator. The ion is laser-cooled to the Lamb–Dicke regime, confining its spatial wave packet to a region much smaller than the optical wavelength. We detect the coupling of ion and fundamental TEM_{00} cavity mode by injecting a light field at 729 nm into the cavity and recording the excitation on the $S_{1/2} \leftrightarrow D_{5/2}$ transition. The excitation probability is monitored via the electron-shelving technique [16, 19], i.e. by probing the fluorescence on the $S_{1/2}- P_{1/2}$ dipole transition (see Fig. 1).

The following stabilized laser sources are used in the experiment: two cavity-locked diode lasers at 866 nm and 854 nm with line widths of ≈ 10 kHz and two Ti:Sa lasers at 729 nm ($\approx$ 1-kHz line width) and 794 nm ($<$ 300-kHz line width), of which the 794-nm laser is resonantly frequency-doubled to obtain 397 nm. The whole laser system is described in more detail elsewhere [3].

The experimental setup of trap and cavity is schematically shown in Fig. 2. The three-dimensional RF Paul trap consists of an elliptical ring electrode with average diameter of 1.4 mm and two end caps with a spacing of 1.2 mm (material: 0.2-mm molybdenum wire). The secular frequencies $(\omega_x, \omega_y, \omega_z)$ are $2\pi \times (2.9, 3.9, 7.4)$ MHz at a RF drive field power of 1 W. Here, z denotes the direction of the trap axis, which is at 45° to the cavity axis. The x and y radial directions both include an angle of $\approx 45°$ with the plane spanned by the cavity and the trap axis. A magnetic field of 3 G perpendicular to the cavity axis provides a quantization axis and a frequency splitting of Zeeman components of the $S_{1/2} \leftrightarrow D_{5/2}$ transition. Calcium ions are loaded into the trap from a thermal atom beam by a two-step photoionization process using diode lasers near 423 nm and 390 nm [20]. The trap is placed in the center of a near-confocal resonator with finesse $\mathcal{F} = 35\,000$ at 729 nm, waist radius $\omega_0 = 54\,\mu$m, mirror separation $L = 21$ mm and radius of curvature $R_M = 25$ mm. Cylindrical piezoceramics (PZTs) allow fine tuning of the cavity length across approximately 1.5 free spectral ranges. In the following this cavity is denoted as the 'trap cavity'.

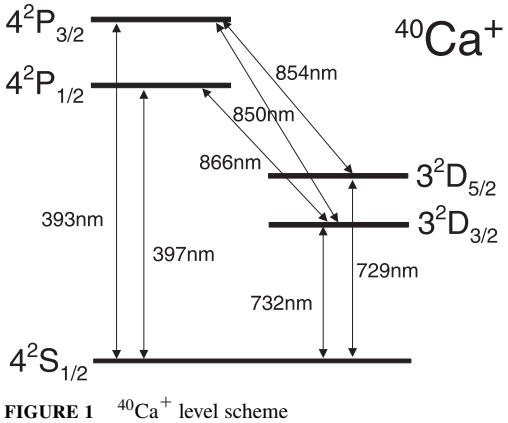

FIGURE 1 $^{40}Ca^{+}$ level scheme

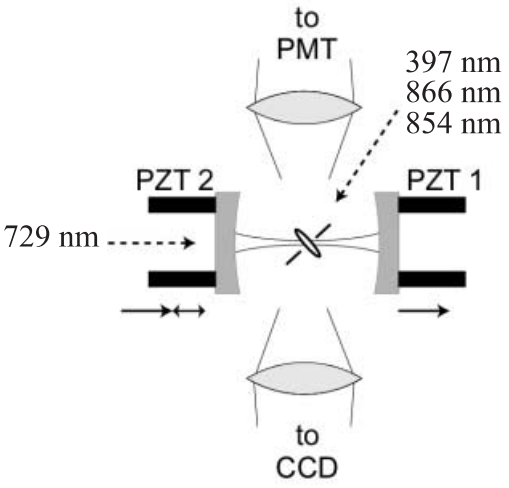

FIGURE 2 Schematic experimental setup. PZT1 denotes the offset piezo, PZT2 the scan piezo. A photomultiplier tube (PMT) is used to record fluorescence on the $S_{1/2}-P_{1/2}$ transition and the CCD camera monitors the ion's position. The *dotted arrows* indicate directions of laser beams: a 729-nm excitation laser along the direction of the cavity axis and a 397-nm cooling laser, 854-nm and 866-nm auxiliary lasers at a certain angle to the trap axis (only shown schematically)

The ion can be excited by a traveling wave using a free 729-nm laser beam at a certain angle to the cavity axis or by the SW built up in the cavity after injecting a 729-nm laser beam into the cavity mode. The position of the ion relative to nodes and anti-nodes of the SW can be controlled by adjusting the offsets of both PZTs.

2.2 *Frequency stabilization of the trap cavity*

In order to study stationary coherent interaction of an atom and a cavity mode it is necessary to stabilize the cavity resonance frequency to the atomic transition frequency. In order to avoid that resonant light present in the cavity perturbs the controlled atom–cavity interaction, we use a 785-nm diode laser for the stabilization, this being far off-resonant to transitions at 729 nm. The basic scheme of the transfer lock is as follows: we frequency lock the 785-nm diode laser to the same ultra-stable reference cavity (see [3]) as the 729-nm Ti:Sa laser. By stabilizing the trap cavity to the diode laser frequency, the lengths of the reference and the trap cavity are fixed relative to each other. Furthermore, the length of the trap cavity is fixed relative to the wavelength of the 729-nm Ti:Sa laser. By applying an appropriate frequency shift to the diode laser, the length of the trap cavity is adjusted to achieve resonance for 729 nm.

Figure 3 illustrates the setup of the diode laser at 785 nm and its stabilization to the reference cavity. The single-mode laser diode (80-mW maximum output power) is temperature-stabilized to a few millikelvin. An external holographic grating with 1800 lines/mm in Littrow configuration creates an extended tuneable resonator. The grating is mounted on a precision mirror holder; fine tuning is achieved by a PZT. The elements described so far are enclosed in a stable aluminum case kept at a constant temperature of (20 ± 0.1) °C by circulating water. After passing through an optical diode with 60-dB isolation the light is split by a polarizing beam splitter. The part of the light being used for the Pound–Drever–

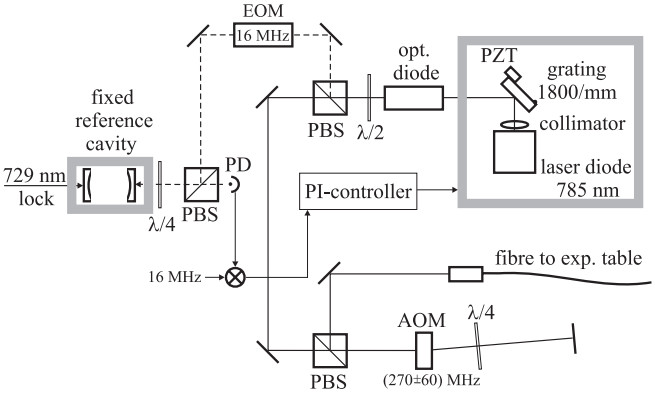

FIGURE 3 Setup of the 785-nm diode laser with extended cavity (Littrow configuration) and frequency stabilization to the reference cavity. The laser beam (≈ 35 mW) is split into a lock beam (≈ 2 mW, *dashed line*) and an experiment beam that is frequency-shifted in a double-pass configuration (*solid line)*. Laser line width: $\Delta\nu_{785} = (1.8 \pm 0.1)$ kHz. For more details see text

Hall lock [21] to the reference cavity (FSR = 750 MHz) is phase-modulated with an electro-optical modulator (EOM) at 16 MHz. The error signal is fed to a PI controller acting on the laser diode current (fast branch) as well as on the grating PZT (slow branch). The light not used for the lock is directed through an acusto-optical modulator (AOM) (double pass), allowing for a continuous frequency shift of approximately ±120 MHz, and is sent to the trap cavity via an optical fiber.

Figure 4 shows the setup of the trap cavity lock to the diode laser at 785 nm. The stabilized 785-nm light leaving the optical fiber is phase-modulated by an EOM at 16 MHz and is coupled into the trap cavity (from the right in Fig. 4) via a polarizing beam splitter. The 729-nm light is coupled into the cavity from the opposite side (left in Fig. 4). On the right-hand side of the cavity, the light is dispersed by a grating (1200 lines/mm) to separate the 785-nm reflected light from the 729-nm transmitted light, which is monitored by a CCD camera and a photodiode. The first-order grating reflection at 785 nm is focused onto a fast photodiode to obtain a Pound–Drever–Hall error signal after mixing with the modulation frequency. The error signal is processed in a PI controller acting on one of the trap-cavity PZTs. On the left-hand side, again a grating is used to separate the transmitted 785-nm light from the reflected 729-nm light. The 785-nm transmission is monitored on a CCD as well as on a photodiode.

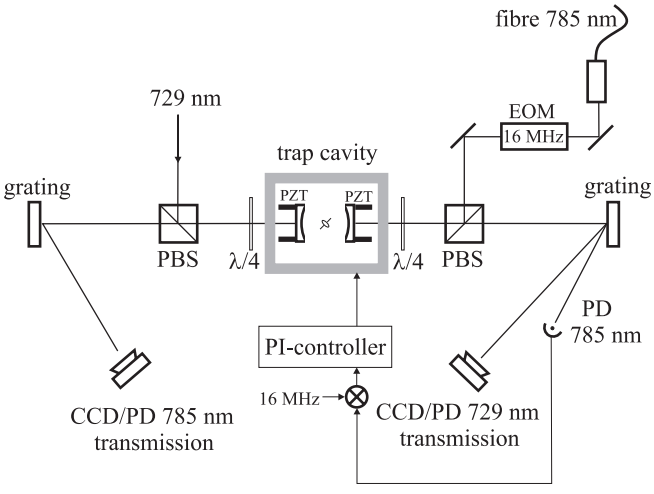

FIGURE 4 Setup of the trap-cavity lock. The light at 785 and 729 nm is coupled into the cavity from opposite directions. Gratings (1200 lines/mm) on both sides separate the beams and ensure clear control of the transmissions on both wavelengths without perturbation by reflections of the other light. For more details see text

The experimental procedure to achieve double resonance of the trap cavity is as follows: by scanning the trap cavity, transmission on the 729-nm TEM_{00} mode is recorded. Now the wavelength of the diode laser has to be chosen in such a way that the 785-nm light is also resonant for both the reference and the trap cavities within the range of ±120 MHz, this being covered by the double-pass AOM. Usually, this can be achieved by current tuning the diode to one of its longitudinal modes.

3 Experiments on ion–cavity coupling

In the following, we report four different experiments exploring various aspects of the ion–cavity coupling: First, we probe the ion's response to temporal variations of the cavity internal field by scanning the cavity over the resonance with the incident laser light, thus imprinting a phase and amplitude modulation on the cavity field [22, 23]. Second, using the same scanning excitation technique we detect the ion's response to spatial variations of the intracavity SW field (mapping of the longitudinal field distribution). Third, we investigate coupling of the ion's vibrational modes to the cavity field by comparing the excitation on the carrier transition and on the first vibrational sideband at different positions in the SW. Finally, we observe coherent interaction of ion and cavity field by exciting Rabi oscillations with short resonant laser pulses coupled into the frequency-stabilized cavity.

3.1 *Measurement procedures*

The general procedure for all experiments is the following:

- The ion is Doppler-cooled and prepared in the electronic ground state.
- A sequence of laser pulses is applied to the ion.
- The final electronic state is detected.

These three steps are described in detail in the following (cf. Fig. 5).

First, the ion is Doppler-cooled for 1.9 ms on the $S_{1/2}$–$P_{1/2}$ transition. During cooling the 854-nm laser is switched on to remove any population in the metastable $D_{5/2}$ state. In addition, we irradiate the ion with a laser beam at 866 nm at all times to prevent shelving in the metastable $D_{3/2}$ state. From coherent dynamics (Rabi oscillations) on the carrier and first motional sidebands [16], we determine typical mean vibrational quantum numbers after Doppler cooling $(\bar{n}_x, \bar{n}_y, \bar{n}_z) = (20 \pm 5, 4 \pm 1, 6 \pm 1)$. From these mean phonon numbers and the secular frequencies given in Sect. 2.1 we calculate a rms extension of the ion's motional wave packet of (25 ± 5) nm in the direction of the cavity axis, much smaller than the wavelength of 729 nm. At the end of the cooling sequence the ion is optically pumped into the $S_{1/2}\,(m = -1/2)$ Zeeman sub-level

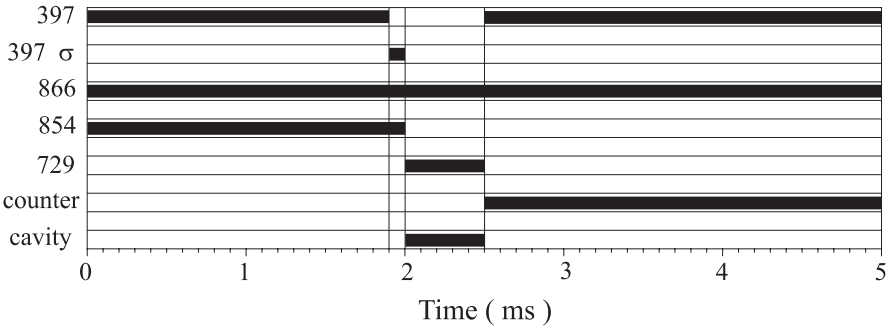

FIGURE 5 Example of a 5-ms pulse sequence. In the first 2 ms a defined 'starting' state is prepared. Then this state is manipulated (2 ms to 2.5 ms). Finally the outcome is detected (excitation or not) for the remaining time. The 10-ms and 20-ms pulse sequences differ only in a longer manipulation window (up to 3 ms) and a longer detection time

by applying a 0.1-ms σ^--polarized pulse at 397 nm. After that, all light at 397 nm is switched off.

Second, the ion is excited on the $S_{1/2} \leftrightarrow D_{5/2}$ ($m = -1/2$ to $m' = -5/2$) transition by a free laser beam or by light resonant in the trap cavity. A time window of 0.5 to 3 ms is assigned to this process. Interaction of the ion and light within the trap cavity can be achieved by either frequency locking the cavity to the quadrupole transition or by a cavity scanning technique. In the first case we inject short resonant laser pulses with variable pulse length into the frequency-stabilized cavity in order to study coherent ion–field interaction. The second technique is used for investigating the ion's response to dynamical or spatial variations of the intracavity field. Here, the laser at 729 nm is set to a fixed detuning Δ from the $S_{1/2} \leftrightarrow D_{5/2}$ transition. We inject the laser beam into the cavity TEM_{00} mode (cf. Fig. 4) and apply a voltage ramp to the scan PZT in order to scan the cavity length. When the cavity reaches resonance with the laser frequency it fills with light and may excite the ion to the $D_{5/2}$ level. Then the light at 729 nm is switched off and the cavity mirror is ramped down to its initial position.

Third, we determine the excitation probability via the electron-shelving technique. The blue light at 397 nm is switched on (866-nm light is on anyway) and the fluorescence is counted by the PMT for a time interval between 2.3 ms and 17 ms depending on the duration of the total pulse sequence (5, 10 or 20 ms). The PMT count rate for the fluorescent ion is ≈ 16 kHz; the signal-to-background ratio ~ 10. By comparing the number of counts in the time interval with a threshold we can discriminate with very high probability ($> 99\%$) [16] whether excitation happened (electron shelved in $D_{5/2}$, no fluorescence) or the ion remains in the ground state (fluorescence). Note that although state detection happens a few ms after the ion–light interaction the ion's state is well preserved due to the long lifetime (1 s) of the $D_{5/2}$ level.

All three steps are typically repeated 100 times to yield the average excitation probability. After that, changes in the excitation window may be applied, such as a change in the laser frequency (frequency scan) or a change in the excitation pulse length (pulse-length scan). For example, to obtain an excitation spectrum, the 729-nm laser is tuned over the quadrupole transition in steps of 1 kHz.

3.2 *Temporal variation of the intracavity field*

In our first experiment we probe the ion's response to temporal variations of the intracavity field by placing it close to a node of the SW field [24] and varying the cavity scan rate.

Figure 6 shows the excitation probability on the $S_{1/2} \leftrightarrow D_{5/2}$ transition for different scan rates. For negative (positive) scan rates the mirrors move towards each other (apart) and thereby Doppler shift the light to the blue (red). The atomic transition then seems to be red (blue)-shifted as the excitation laser detuning has to compensate for the Doppler shift. Increasing scan rate increases the shift from the line center (detuning zero), which is found by excitation with a free laser beam. In addition, faster scan rates broaden the line because more and more frequency components are added to the light confined in the cavity.

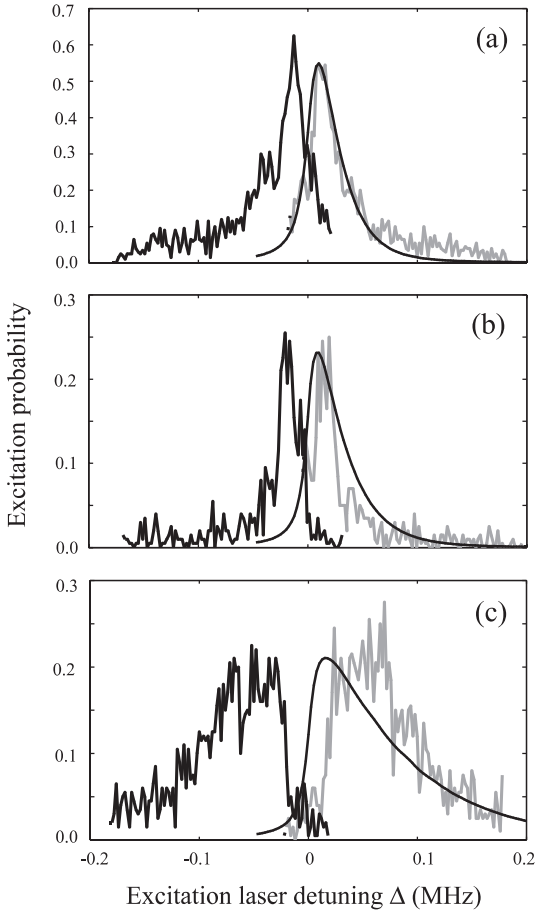

FIGURE 6 Excitation spectra for different cavity scan rates $\nu_L = \pm 0.16$ (**a**), ± 0.23 (**b**) and ± 0.69 (**c**). On the blue-shifted spectra (*gray lines*), theoretical simulations are superimposed (*solid line*). The parameters for the simulations are: laser bandwidth $\Delta\nu_{\text{laser}} = 6$ kHz, natural line width of the $S_{1/2} \leftrightarrow D_{5/2}$ transition $\Delta\nu_{\text{SD}} = 0.17$ Hz, Rabi frequency for zero detuning: $\Omega_0 = 15.5$ kHz (**a**), 11 kHz (**b**) and 25 kHz (**c**)

To put these observations in a more quantitative form it is convenient to define a normalized scan rate $\nu_L = 2\mathcal{F}\omega\dot{L}\tau/(\pi c)$. It corresponds to the resonance frequency shift of the cavity in units of the HWHM cavity line width $c/(4L\mathcal{F})$ per cavity energy storage time $\tau = \mathcal{F}L/(\pi c)$. To model the coupling dynamics we first have to know the electric field acting on the ion. The electric field amplitude E_{cav} in a cavity swept over resonance is a solution of the differential equation [22, 23]:

$$\frac{\mathrm{d}E_{\mathrm{cav}}}{\mathrm{d}\bar{t}} = -(1 - \mathrm{i}\nu_L\bar{t})E_{\mathrm{cav}} + \mathrm{i}\frac{\sqrt{T}\mathcal{F}}{\pi}E_0\,,$$

where $\bar{t} = t/\tau$, $T \approx \pi/\mathcal{F}$ is the transmission of the input coupling mirror and E_0 is the amplitude of the input field. For slow scan rates ($\nu_L \ll 1$) we obtain the quasi-static case, whereas for fast scan rates ($\nu_L \gg 1$) the incoming light interferes with the light stored in the cavity. Figure 7 shows the normalized intracavity field amplitude for three different scan rates.

The interaction of this time-dependent electric field with the ion can now be modeled by numerically integrating the Bloch equations for a two-level system. The result for a scan rate of $\nu_L = 1$ and a typical laser intensity is shown in Fig. 8. The electronic transition (Fig. 8, top) is blue-shifted and broadened compared to the excitation with a free laser beam, as expected.

Figure 8 (bottom) illustrates, for five different detunings Δ, the time evolution of the excitation to the $D_{5/2}$ level as the cavity is swept over resonance. For all detunings, the excitation probability shows a steep rising edge at the moment the cavity fills with light and subsequent Rabi oscillations with a damping depending on excitation power and detuning. This excitation characteristic remains qualitatively unchanged over a large range of excitation powers and scan rates. The final stationary values of the excitation probabilities are taken to compose the excitation spectrum (Fig. 8, top).

The results of the theoretical simulation for positive scan rates are shown as solid lines superimposed on the blue-shifted spectra in Fig. 6. The calculated and experimental spectra show good agreement for small scan rates (Fig. 6a,b).

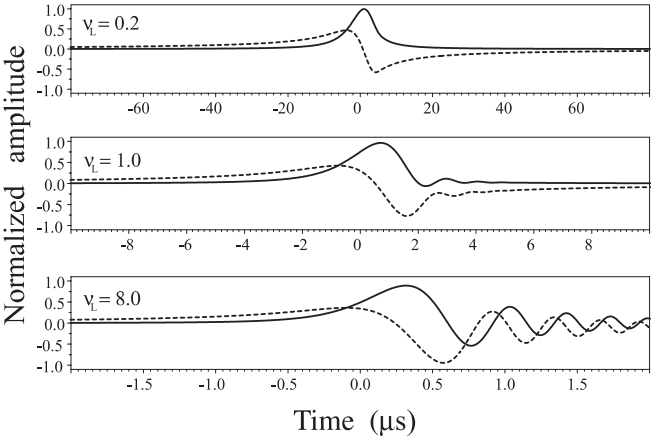

FIGURE 7 Calculated time-dependent normalized electric field amplitude in the cavity for three different scan rates ν_L. The *solid line* is the real part; the *dashed line* the imaginary part of the electric field amplitude. For large scan rates the interference of incoming and stored light becomes visible

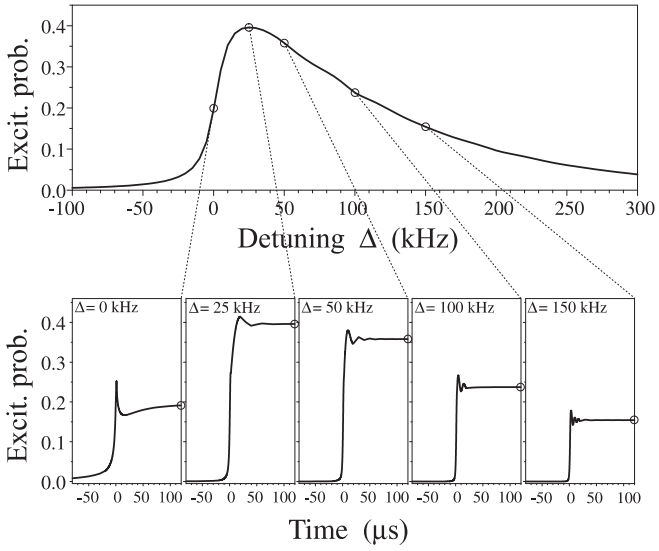

FIGURE 8 Simulated excitation spectrum for $\nu_L = 1$ (*top*) and time evolution of the excitation probability for different detunings Δ (*bottom*). More details are given in the text

For larger scan rates (Fig. 6c) the centers of the spectra are slightly shifted. We assume that this shift is caused by nonlinearities and hysteresis effects of the PZT motion. Although we kept the excitation power constant in the experiments, we left the Rabi frequency Ω_0 as a fitting parameter to account for variations in excitation due to thermal drift of the cavity shifting the node of the SW away from the ion's position.

The investigation and theoretical understanding of the ion–cavity field coupling dynamics as discussed above are important for realization of the atom–photon interface in quantum networks. The experimental implementation of such a scheme requires control over the shape of the light pulse emitted from the cavity and thus control over the dynamic atom–cavity coupling [4].

3.3 *Spatial variation of the intracavity field*

The trapped single ion is confined to a region in space of less than 30 nm, which is much less than the excitation wavelength (729 nm). It thus can be used as a nanoscopic probe of the SW field spatial variation as first shown in [6, 25]. To probe this spatial variation, we again use the cavity scanning technique and leave the scan rate fixed at a small value, allowing for stable scans with only a little perturbation of the excitation spectrum as in Fig. 6a. The laser is scanned over the quadrupole transition in steps of ~ 1 kHz to obtain an excitation spectrum at a certain position in the SW. To use the excitation probability as a measure of the field intensity, it is important to adjust the laser power such that the excitation is kept well below saturation at all positions in the SW. The offset voltage of both scan PZT and offset PZT is then varied simultaneously in such a way that the SW in the cavity is shifted longitudinally with respect to the location of the ion. Repetition of the procedure yields a number of excitation spectra shown in Fig. 9. The position-dependent excitation probability is determined by fitting each excitation spectrum with a Lorentzian and adopting the peak value. Figure 10 displays these values as a function of the PZT offset voltage.

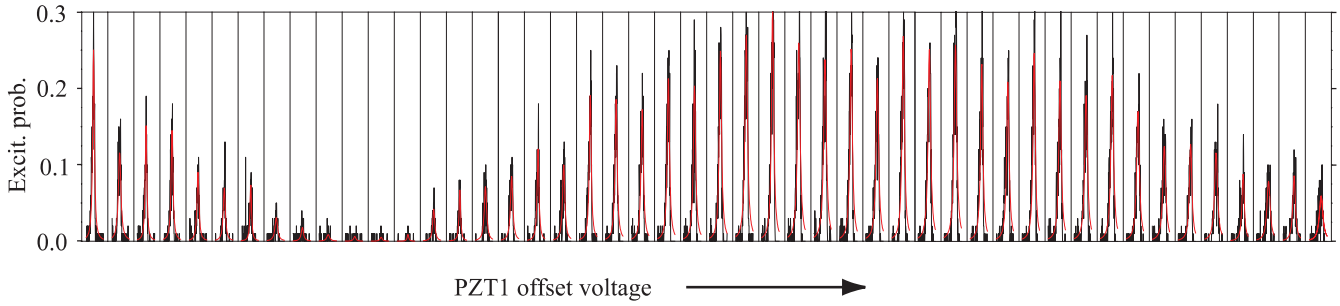

FIGURE 9 All 48 excitation spectra measured at different positions in the intracavity SW. Every box (width: 600 kHz) contains a spectral line as in Fig. 6; the offset voltage increases from *left* to *right*. The SW pattern is already visible; the total shift is ∼ 1.5 half-waves

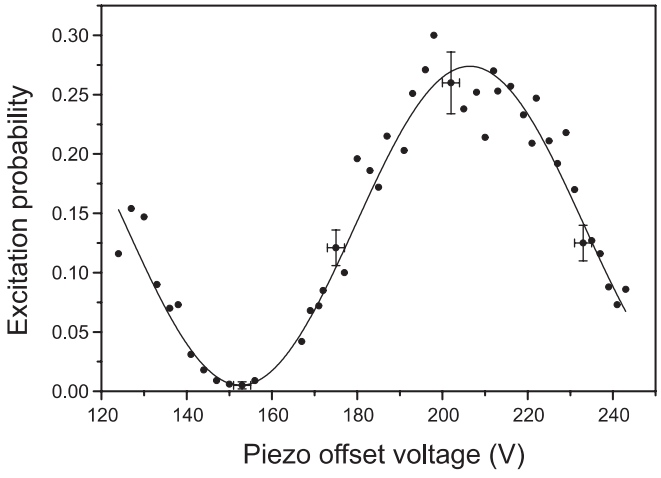

FIGURE 10 Excitation probability on the $S_{1/2} \leftrightarrow D_{5/2}$ transition of a single trapped Ca^+ ion as a function of the PZT offset voltage, i.e. at various positions in the intracavity standing wave field. The *solid line* represents a $\sin^2$ function fitted to the data points

Error bars given for representative data points in Fig. 10 are due to PZT hysteresis (abscissa) and the errors of the fits to the excitation spectra (ordinate). The excitation probability varies spatially with the intensity of the SW [24]. A theoretical Bloch-equation analysis as described above predicts a nearly pure $\sin^2$ spatial variation, deviating by less than 1%. From a $\sin^2$ fit to the data points we obtain the contrast ratio (visibility V) of the position-dependent excitation, $V = 96.3 \pm 2.6\%$. This very high visibility results from the strong confinement of the ion's wavefunction. The laser-cooled ion, oscillating with its secular frequencies and with thermally distributed amplitudes, has a rms spatial extension along the cavity axis of a_c. This extension leads to a reduction of the excitation contrast by a factor of $\exp(-2(2\pi a_c/\lambda)^2)$ compared to the excitation contrast experienced by a point-like atom at rest. From the measured visibility V we find $a_c = 16^{+5}_{-7}$ nm. The small value of the extension a_c shows that in this experiment we cool the ion close to the Doppler limit (13 nm).

A necessary condition for all experiments relying on ion–cavity mode coupling is the ability to place the ion at a certain position of the intracavity SW field with high precision and high reproducibility [6]. In our experiment, the precision of positioning the center of the ion's wavefunction, using a measurement as in Fig. 10, is limited by the uncertainty in the measured excitation probability. This uncertainty is due to a statistical error, i.e. the finite number of state-detection measurements, and systematic errors such as fluctuations of laser intensity and wavelength, drift and jitter of the scan PZT, etc. [25]. From the uncertainties in excitation probability (error bars in Fig. 10) we deduce a spatial precision between 7 nm ($\approx \lambda/100$) at the position of largest slope and 12 nm and 36 nm at minimum or maximum excitation, respectively. We note, however, that the precision can be enhanced by averaging over a larger number of state-detection measurements.

3.4 *Coupling of motional states*

Many schemes for quantum information processing with trapped ions rely on coherent interaction not only with the internal state but also with the motional degrees of freedom. A controlled coupling of atomic states dressed by vibrational modes to the cavity field is a precondition for realizing such schemes.

If one compares carrier (no change of vibrational quantum number, $\Delta n = 0$) and first vibrational sideband ($\Delta n = -1$) transition probabilities in a SW, both show a position-dependent coupling due to the SW pattern as shown in Sect. 3.3. But where the coupling to the carrier is strongest, no coupling to the first (i.e. all odd) sidebands occurs and vice versa, i.e. carrier and odd sideband excitations map the SW spatial field variation, but the traces are shifted by a phase factor of π. This phase shift arises due to symmetry characteristics of the transition matrix elements of carrier and sideband transitions in a SW field [1, 12]: the spatial part of the quadrupole transition matrix element is proportional to $\langle n'|\exp(\mathrm{i}kx)|n\rangle$ for a traveling wave (TW) and $\langle n'|\cos(kx)|n\rangle$ for a SW with the electric field $E \propto \sin(kx)$ [24]. Here n and n' are the vibrational quantum numbers in the $S_{1/2}$ and $D_{5/2}$ levels, respectively, k is the wavenumber and x is the ion's position in the field. For a TW, all vibrational states (n, n') can be coupled since $\exp(\mathrm{i}kx)$ contains even and odd powers of kx [26]. In contrast, for a SW $\langle n'|\cos(kx)|n\rangle$ has to be expanded into even *or* odd powers of kx depending on the ion's position, e.g. $x = 0$ close to a node or $x = \lambda/4$ close to an anti-node. Thus, transitions changing the phonon number by even or odd integers can only be excited at different positions in the SW. The first-sideband transition ($\Delta n = \pm 1$) couples maximally at anti-nodes of the SW, whereas the carrier transition ($\Delta n = 0$) couples maximally at nodes. In order to demonstrate this motion-dependent coupling, we recorded excitation probabilities of the ion at a fixed cavity scan rate ($v_L = -0.23$), for different positions within the SW, and with the laser at 729 nm now tuned to either the carrier or the red axial side-

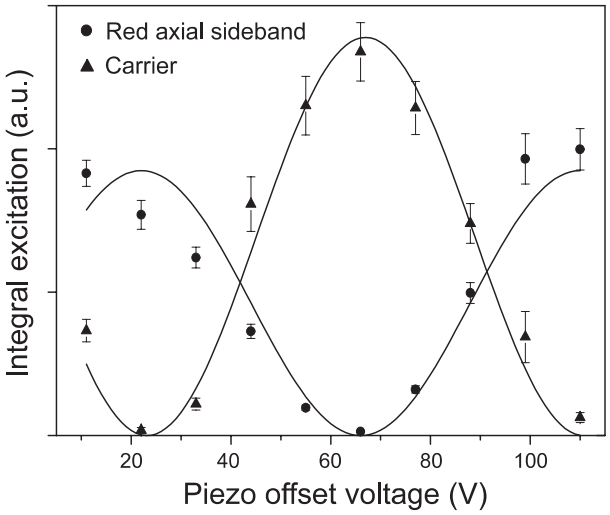

FIGURE 11 Integral excitation on the carrier (*triangles*) and the red axial sideband (*circles*) of the $S_{1/2} \leftrightarrow D_{5/2}$ transition as a function of the PZT offset voltage, i.e. at various positions in the intracavity standing wave field. The *solid lines* represent fits of $\sin^2$ functions to the data points

band ($\Delta n = -1$, laser-detuned by $-\omega_z$) of the $S_{1/2} \leftrightarrow D_{5/2}$ transition. In both cases, the intensity of the laser was adjusted such that the excitations of carrier and sideband were comparable and were kept well below saturation. In this experiment we determine the integral excitation, i.e. the area of the respective excitation spectra, as the spectra show an asymmetric line shape (cf. Fig. 6b,c). The high-contrast orthogonal coupling of carrier and sideband transitions to the cavity mode is demonstrated in Fig. 11.

This coupling facilitates applications such as cavity-assisted cooling in a SW [12], the Cirac–Zoller quantum-computing scheme [27] and entanglement of motional and photonic states when coupling to the cavity vacuum field [17, 18]. In particular, cavity-assisted cooling in a SW field means that sideband cooling [16] on a red-detuned vibrational sideband is facilitated by suppression of off-resonant carrier transitions which induce motional heating. In a similar fashion, unwanted off-resonant carrier excitations are suppressed when driving sideband transitions in the Cirac–Zoller quantum-computing scheme. Here, off-resonant carrier excitations impose a limit on the attainable gate speed [28]. As electronic excitation probabilities of the ion depend on both the vibrational state and the position within the cavity field, the internal electronic degrees of freedom are coupled to both the (in general: quantized) single-mode cavity field and the vibrational degrees of freedom. This coupling allows e.g. for generation of an entangled state of a subsystem that can store quantum information (vibration, electronic states) with a subsystem that can be used for propagation of quantum information (light).

3.5 *Coherent ion-cavity coupling*

The application of the ion–cavity coupling for implementation of quantum network schemes requires a controlled *coherent* interaction. To demonstrate such coherent coupling to the cavity field we stabilize the trap cavity to the $S_{1/2} \leftrightarrow D_{5/2}$ carrier transition frequency as described in Sect. 2.2. We excite the ion with resonant laser pulses of different pulse lengths injected into the trap cavity. Starting from a pulse length of zero up to a pulse of 3-μs duration we determine the average excitation probability from 100 experiments per pulse length. The resulting coherent dynamics (Rabi oscillations) are shown in Fig. 12 together with a numerical simulation (solid line). The theoretical curve is calculated assuming a thermal distribution over harmonic oscillator states $|n\rangle$. The Rabi frequency of any particular $|\mathrm{S}, n\rangle \leftrightarrow |\mathrm{D}, n\rangle$ transition depends on $n\eta^2$, where η is the Lamb–Dicke parameter. The thermal mixture of different oscillation frequencies washes out the Rabi oscillations, which therefore appear damped.

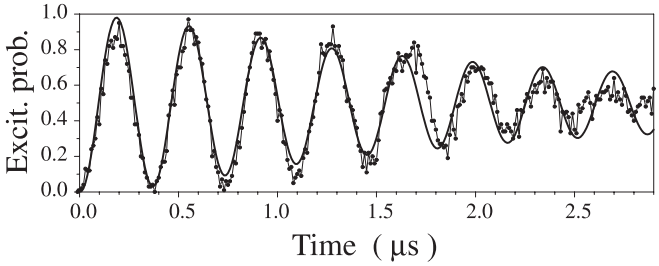

FIGURE 12 Rabi oscillations driven by the light field in the stabilized cavity. The parameters for the theoretical simulation are: Rabi frequency $\Omega_0 = 8.95$ MHz, $\eta^2\bar{n} = 0.049$ and laser detuning $\Delta = 0$

4 Summary and outlook

In summary, we have demonstrated coherent coupling of electronic and motional states of a single trapped ion to a single field mode of a high-finesse cavity. The position of the ion within the standing wave can be determined with a precision of up to $\lambda/100$. As the electronic quadrupole transition in Ca^{+} is one of the candidates for implementing a quantum bit, our experiments are a key step towards realization of quantum computing and communication schemes with trapped ions that require a controlled coherent interaction of ion and cavity field. Future experiments aim at demonstrating and utilizing cavity-modified spontaneous emission for applications such as triggered single-photon emission and realization of the atom–photon interface. Another route is the extension of the current configuration towards trapping of two or more ions coupled to a common cavity mode, thus allowing for implementation of quantum logical gate operations.

ACKNOWLEDGEMENTS This work is supported by the Austrian 'Fonds zur Förderung der wissenschaftlichen Forschung' (SFB15), by the European Commission (TMR networks 'QI' and 'QSTRUCT' (ERB-FRMX-CT96-0087 and -0077), IHP network 'QUEST' (HPRN-CT-2000-00121) and IST/FET program 'QUBITS' (IST-1999-13021)) and by the 'Institut für Quanteninformation GmbH'. C.R. acknowledges support by Fundação para a Ciência e a Tecnologia (Portugal) under the grant SFRH/BD/6208/2001.

REFERENCES

1 M. Šašura, V. Bužek: J. Mod. Opt. **49**, 1593 (2002)
2 W. Paul: Rev. Mod. Phys. **62**, 531 (1990)
3 H.C. Nägerl, Ch. Roos, D. Leibfried, H. Rohde, G. Thalhammer, J. Eschner, F. Schmidt-Kaler, R. Blatt: Phys. Rev. A **61**, 023405 (2000)

4 J.I. Cirac, P. Zoller, H.J. Kimble, H. Mabuchi: Phys. Rev. Lett. **78**, 3221 (1997)
5 A.B. Mundt, A. Kreuter, C. Becher, D. Leibfried, J. Eschner, F. Schmidt-Kaler, R. Blatt: Phys. Rev. Lett. **89**, 103 001 (2002)
6 G.R. Guthöhrlein, M. Keller, K. Hayasaka, W. Lange, H. Walther: Nature **414**, 49 (2001)
7 C.K. Law, H.J. Kimble: J. Mod. Opt. **44**, 2067 (1997)
8 A. Kuhn, M. Hennrich, G. Rempe: Phys. Rev. Lett. **89**, 067901 (2002)
9 K.M. Gheri, C. Saavedra, P. Törmä, J.I. Cirac, P. Zoller: Phys. Rev. A **58**, R2627 (1998)
10 N. Lütkenhaus: Phys. Rev. A **61**, 052304 (2000)
11 E. Knill, R. Laflamme, G.J. Milburn: Nature **409**, 46 (2001)
12 J.I. Cirac, R. Blatt, P. Zoller, W.D. Phillips: Phys. Rev. A **46**, 2668 (1992)
13 E.M. Purcell: Phys. Rev. **69**, 681 (1946)
14 J.I. Cirac, M. Lewenstein, P. Zoller: Phys. Rev. A **51**, 1650 (1995)
15 D.M. Meekhof, C. Monroe, B.E. King, W.M. Itano, D.J. Wineland: Phys. Rev. Lett. **76**, 1796 (1996)
16 Ch. Roos, Th. Zeiger, H. Rohde, H.C. Nägerl, J. Eschner, D. Leibfried, F. Schmidt-Kaler, R. Blatt: Phys. Rev. Lett. **83**, 4713 (1999)
17 V. Bužek, G. Drobný, M.S. Kim, G. Adam, P.L. Knight: Phys. Rev. A **56**, 2352 (1997)
18 F.L. Semião, A. Vidiella-Barranco, J.A. Roversi: Phys. Rev. A **64**, 024305 (2001)
19 H. Dehmelt: Bull. Am. Phys. Soc. **20**, 60 (1975)
20 S. Gulde, D. Rotter, P. Barton, F. Schmidt-Kaler, R. Blatt, W. Hogervorst: Appl. Phys. B **73**, 861 (2001)
21 R.W. Drever, J.L. Hall, F.V. Kowalski, J. Hough, G.M. Ford, A. Munley, H. Ward: Appl. Phys. B **31**, 97 (1983)
22 H. Rohde, J. Eschner, F. Schmidt-Kaler, R. Blatt: J. Opt. Soc. Am. B **19**, 1425 (2002)
23 M.J. Lawrence, B. Willke, M.E. Husman, E.K. Gustafson, R.L. Byer: J. Opt. Soc. Am. B **16**, 523 (1999)
24 Note that the atomic quadrupole moment couples to the gradient of the electric field. The maximum excitation thus occurs at the nodes of the standing wave
25 J. Eschner, C. Raab, F. Schmidt-Kaler, R. Blatt: Nature **413**, 495 (2001)
26 Note that $kx = \eta(a + a^\dagger)$, for the ion oscillating around $x = 0$, where η is the Lamb–Dicke parameter and $a^\dagger$ and a are the phonon creation and annihilation operators, respectively
27 J.I. Cirac, P. Zoller: Phys. Rev. Lett. **74**, 4091 (1995)
28 A. Steane, C.F. Roos, D. Stevens, A. Mundt, D. Leibfried, F. Schmidt-Kaler, R. Blatt: Phys. Rev. A **62**, 042305 (2000)